Upconverter-Powered Oxygen Sensing in Electrospun Polymeric Bilayers

Kayla F. Presley,[a] Soshan Cheong,[b] Alex Cochran,[a] Richard D. Tilley,[b] Josh E. Collins,[c] John J. Lannutti[a]
[a]Department of Materials Science and Engineering, The Ohio State University, Columbus, OH 43210, USA
[b]School of Chemistry, UNSW Australia, Sydney NSW 2052, Australia
[c]Intelligent Materials Solutions, Inc., Princeton, NJ 08540

Abstract: Optical oxygen sensors based on luminescent quenching are attractive as they are easily miniaturized, offer excellent sensitivity, and in the appropriate vehicle exhibit no cytotoxicity. However, these sensors must be energized by violet or blue wavelengths to report variations in oxygen content. These wavelengths experience high levels of absorption and scattering in biological tissue. Upconverting particles (UCPs) sidestep this limitation due to their ability to sequentially absorb two or more longer wavelength photons to emit a single, shorter wavelength photon. In this work, UCPs were utilized to emit blue light upon near infrared (NIR) absorption. A key advantage is that NIR light efficiently penetrates tissue barriers associated with potential biomedical applications. A layer of polycaprolactone (PCL) fibers containing $Ru(dpp)_3Cl_2$ was electrospun directly on top of a layer of fibers containing UCPs. We chose a bilayer configuration as it allowed direct examination of the 'handshake' interaction and investigation of significant design issues. Configurational aspects of the bilayer format were studied. Additionally, gaseous oxygen sensing following NIR excitation was confirmed. These upconverter-powered sensors were found to have a rapid response (<0.25 s).

Abbreviations: upconverting particles (UCPs); near infrared (NIR); polycaprolactone (PCL); scanning electron microscopy (SEM); x-ray diffraction (XRD); tris (4,7-diphenyl-1,10-phenanthroline) ruthenium (II) dichloride ($Ru(dpp)_3Cl_2$); 1,1,1,3,3,3-hexafluoro-2-propanol (HFP); energy dispersive x-ray spectroscopy (EDS); phosphate-buffered saline (PBS); photomultiplier tube (PMT); polyethersulfone (PES)

1. Introduction

The ability to sense and report localized oxygen content in biological environments is greatly desired in many biomedical applications. Oxygen is of vital importance for many cellular processes having biological significance.[1] For instance, oxygen supply is a crucial limiting factor during three-dimensional cell culture directed toward tissue engineering.[2] In addition, cancerous tumors possess highly heterogeneous levels of oxygen, and cells residing within hypoxic regions characterized by extremely low oxygen concentration better resist radiation and chemotherapy.[3,4]

The biophotonic reporting of oxygen content in biological environments is desired for both *in vitro* and *in vivo* (i.e., under-the-skin) applications. Thus, optical oxygen sensors based on luminescent quenching phenomena are attractive for these applications as they are easily miniaturized and show many desirable properties, including rapid response, decreased toxicity and improved sensitivity.[5] Additional advantages include their lack of oxygen consumption and freedom from electrical interference.[6] In general, sensor luminescence is dynamically quenched by molecular oxygen, the degree of quenching corresponding to the amount of oxygen present.[7]

The most widely used luminescent oxygen-sensitive molecules are considered to be palladium (II) and platinum (II) tetrakis(pentafluorophenyl)porphyrin (PdTFPP and PtTFPP, respectively) and tris (4,7-diphenyl-1,10-phenanthroline) ruthenium (II) dichloride ($Ru(dpp)^{3+}$).[8] Compared to PtTFPP, PdTFPP exhibits a longer lifetime (1.65 ms versus 60 μs) and an improved quantum yield (0.21 versus 0.088).[9,10] Although $Ru(dpp)^{3+}$ has a shorter lifetime (6.4 μs), it exhibits a good quantum yield (0.366) and has the advantage of a broad absorption spectrum in the visible region.[11] To create a functional sensor, oxygen-sensitive molecules are generally dispersed throughout a polymer host, generally in the format of a thin film. The host is selected for its optical properties and oxygen permeability and must also be an acceptable solvent for the oxygen-sensitive molecules.[6] Silicone rubbers and poly(1-trimethylsily-1-propyne) are sometimes used due to their excellent oxygen permeability.[12,13] Other common choices include polymers with moderate oxygen permeability but improved mechanical properties, such as polystyrene (PS).[14,15] There have been numerous recent advances in biological detection by luminescent oxygen sensing. Recent efforts often either use two-photon microscopy[16,17] for increased penetration or phosphorescence lifetime imaging [18,19] for improved measurement robustness. Additionally, there have been promising advancements in the area of intracellular oxygen measurements [20,21] and 3D tissue models.[18] To accomplish intracellular oxygen measurements, the use of nanoparticles is often employed.[17]

However, these sensors commonly rely on visible wavelengths to report variations in oxygen content. This can compromise their ability to transmit information through either adherent cell layers or tissue. The ability of light to travel through biological tissue is a function of absorption and scattering, both of which are strongly wavelength dependent.[22] In fact, the range of 600-1300 nm is referred to as the “optical window.”[23] Depth of penetration at lower wavelengths is limited by strong absorption from pigments, such as melanin and hemoglobin, while higher wavelengths are strongly

absorbed by water.[23,24] Additionally, Rayleigh scattering is reduced as wavelength increases.[25] Therefore, compared to visible light, near-infrared (NIR) light can penetrate tissue to much greater depths with minimal damage.[23]

How can we utilize NIR to stimulate oxygen-sensitive molecules that are only excited by 480 nm wavelengths? Upconverting particles (UCPs), such as lanthanide-doped crystals, meet this need due to their ability to sequentially absorb two or more photons and then emit a single *shorter* wavelength photon.[26,27] More specifically, these materials can be made to emit visible light after NIR absorption.[26] For instance, specific crystals, such as Y_2O_2S or $NaYF_4$, doped with the sensitizer ion Yb^{3+} and the emitter ion Tm^{3+}, emit blue light (480 nm) upon 980 nm NIR excitation. As before, the key overall advantage is that NIR light efficiently penetrates soft tissues and cell layers associated with potential biomedical applications.[28] Fortunately, these upconverting particles exhibit low cytotoxicity and have already been utilized *in vivo*.[26] They exhibit high signal-to-noise ratios, a lack of background autofluorescence, elevated photostabilities and long lifetimes.[27–29]

In this work, we studied the idea of a 'handshake' interaction between upconverting particles and oxygen-sensitive molecules. We use the term 'handshake' to refer to the *local* stimulation of these oxygen-sensitive molecules by the UCPs following *external* NIR excitation. This is in contrast to luminescence resonance energy transfer (LRET) that only occurs if the UCPs and Ru complex are very close to one another (i.e., within 10 nm).[30] Specifically, by using Y_2O_2S:Yb,Tm upconverting particles in conjunction with $Ru(dpp)_3Cl_2$, we wished to make use of the "optical window" as a means of extending the oxygen sensing capabilities of $Ru(dpp)_3Cl_2$ to a wider range of biological applications. Due to its ability to easily penetrate soft tissues and cell layers with minimal damage, a 980 nm NIR laser is used as the excitation source for UCPs. The UCPs' subsequent blue emission (480 nm) then excites the oxygen-sensitive molecules, which emit a red luminescence (625 nm) dynamically quenched by oxygen. Figure 1A demonstrates the detailed energy transfers involved in this process. Despite the advantages of PdTFPP and PtTFPP, $Ru(dpp)_3Cl_2$ was chosen due to the large spectral overlap between its broad visible absorption spectra and the upconverter emission.

The specific form used involves the electrospun bilayers shown in Figure 1B. A layer of nanofibers containing $Ru(dpp)_3Cl_2$ is electrospun directly on top of a layer of nanofibers containing UCPs. We chose a bilayer configuration as it allows direct study of the 'handshake' interaction and of significant design issues that can be more readily addressed using this form. Additionally, thin bilayers have been utilized in many sensing applications (i.e., for glucose, hydrogen gas and amine vapor sensing).[31–33] We decided to construct each layer out of electrospun nanofibers instead of polymer films to achieve rapid response times characteristic of the shorter diffusion distances and enhanced surface-to-volume ratio.

Here, we utilize a combined experimental and analytical approach to analyze these electrospun bilayer sensors. Such an approach was used to develop an understanding of the 'handshake' interaction and its relation to morphology as well as to confirm the

function of the sensor. We employed x-ray diffraction (XRD) to verify the presence of the UCPs in the electrospun fibers, while scanning electron microscopy (SEM) was necessary to study the distribution of the UCPs within the bilayer structure. Confocal luminescence was needed to confirm the 'handshake' and image it on a local level. Meanwhile, the actual performance of the sensor was evaluated via spectroscopic techniques to measure the response time and evaluate whether it could be used for gaseous oxygen sensing.

2. Materials and Methods

2.1 Materials

Y_2O_2S:Yb,Tm microparticles were obtained from Intelligent Material Solutions (Princeton, NJ, USA). Tris (4,7-diphenyl-1,10-phenanthroline) ruthenium (II) dichloride ($Ru(dpp)_3Cl_2$) was acquired from Frontier Scientific (Logan, UT, USA). Polycaprolactone pellets (PCL, M_n: 70,000–90,000) were purchased from Sigma-Aldrich (St. Louis, MO, USA). The solvent 1,1,1,3,3,3-hexafluoro-2-propanol (HFP) was obtained from Oakwood Products (West Columbia, SC, USA).

2.2 Fabrication of electrospun bilayers

To prepare the oxygen complex-containing solution, sufficient PCL pellets were first added to HFP to form a 5 wt% solution. $Ru(dpp)_3Cl_2$ was then added to this solution at a ratio of 5 mg Ru complex:1 g PCL. The upconverting particle solution was created in a similar manner. Y_2O_2S:Yb,Tm particles were added to a 5 wt% PCL in HFP solution at a ratio of 80 mg UCPs:1 g PCL. These solutions were stirred with a magnetic stirrer for 3 hours at 60 rpm until the polymer was completely dissolved.

The solutions were electrospun using a 20 gauge needle and a flow rate of 5 mL/hour. The applied voltage was 25 kV, and the needle-to-collector distance was 20 cm.[34] In each case, an approximately 90 μm-thick layer of PCL + Y_2O_2S:Yb,Tm was electrospun. Then, individual layers of PCL + $Ru(dpp)_3Cl_2$ were directly electrospun onto this original layer at thicknesses of ~9, 30, 90 and 270 μm.

This same process was followed to produce a bilayer specimen containing smaller Y_2O_2S:Yb,Tm microparticles and a ~30 μm-thick PCL + $Ru(dpp)_3Cl_2$ layer. These microparticles were produced by grinding the original Y_2O_2S:Yb,Tm microparticles with a vibratory Micro Mill Pulverisette 0 (Fritsch Idar-Oberstein, Germany) for 3 hours. These particles were then heated for an additional 3 hours at 550°C and are subsequently referred to as "ground and annealed" particles.

All bilayer scaffolds were placed under vacuum for 3 hours to remove any residual solvent.[35] The samples were stored under conditions of darkness inside a desiccator.

2.3 Measurements

Fiber morphology and microparticle distribution were examined using a JEOL (Tokyo,

Japan) 6500F field emission SEM at 15 keV equipped with energy dispersive x-ray spectroscopy (EDS). The luminescence of the electrospun scaffolds was analyzed via a JAZ spectrometer from Ocean Optics Inc. (Dunedin, FL, USA). The excitation source used was an adjustable power 980 nm continuous wave diode laser from Dragon Lasers (Changchun, China) set at 1.25 W. The samples were tested in transmission. 0.8 by 1.2 cm bilayer fiber mats were placed in cuvettes with the UCP-containing side facing the laser, while the $Ru(dpp)_3Cl_2$-containing side faced the spectrometer probe. Spectra from each scaffold under pure nitrogen and oxygen conditions were obtained. Response time was examined by switching between oxygen and nitrogen gas every 20 seconds. During this process, the intensity of the emission $Ru(dpp)_3Cl_2$ peak versus time was recorded. The N_2 to O_2 and O_2 to N_2 response times were then calculated. Photobleaching was monitored by recording the emission versus time for one full hour of continuous illumination. This assessment was carried out under blue light excitation and in phosphate-buffered saline (PBS). For gaseous oxygen sensing, the desired oxygen/nitrogen mixture was flowed into the cuvette using a multi-gas proportioning flow meter from Aalborg (Orangeburg, NY, USA), and bilayer luminescence was monitored using the spectrometer.

XRD was performed with a Bruker (Madison, WI, USA) D2 Phaser Powder Diffractometer to establish the presence of the microparticles within the electrospun fiber along with the effects of grinding and annealing on the microparticles. Confocal photoluminescence images were taken using a Leica (Buffalo Grove, IL) TCS SP5 inverted Confocal and Multiphoton Microscope (Mannheim, Germany) equipped with a Spectra-Physics Mai Tai HP 2-photon excitation laser (Mountain View, CA) tunable from 720 –1040 nm. The photomultiplier tube (PMT) detectors were tuned to detect +/- 20 nm around the desired peak emissions of 480 and 630 nm.

3. Results

3.1 X-ray diffraction

Figure 2 shows the XRD patterns for electrospun PCL fibers containing UCPs, while the insets compare XRD patterns for as-received versus ground and annealed UCPs. The crystalline Y_2O_2S:Yb,Tm particles were successfully incorporated into the electrospun PCL fibers where they maintained their crystallinity. Additionally, the inset shows the broadened peaks of the ground and annealed UCPs that result from crystallite size reduction via grinding. However, another possible factor contributing to the broader peaks is the introduction of strain into the system, possibly introducing a strain-broadening effect. There is also a noticeable peak shift potentially attributable to this induced strain.

3.2 Morphology and particle dispersion

SEM characterization of the composition and morphology of an electrospun bilayer specimen is shown in Fig. 3A. The $Ru(dpp)_3Cl_2$-containing layer rests directly on top of the Y_2O_2S:Yb,Tm-containing layer. The visible delamination between the layers is a result of incidental shearing during sample preparation. As expected, the EDS maps (Fig.

3B) reveal the presence of yttrium and sulfur only in the upconverting particle layer, because these elements are present only within the Y_2O_2S:Yb,Tm UCPs. Figs. 4C-D provide a closer look at the PCL + Y_2O_2S:Yb,Tm layer. The secondary electron SEM image (Fig. 3C) demonstrates morphology typical of electrospun fibers. The backscattered electron image of the same area (Fig. 3D) offers specific compositional contrast clearly indicating the presence of Y_2O_2S:Yb,Tm particles.

3.3 Confocal luminescence results

Confocal luminescence results of a bilayer specimen are shown in Figure 4. The output of the aggregated Y_2O_2S:Yb,Tm UCPs following 980 nm excitation produces localized areas of 480 nm emission visible in the grey-scale image (Fig. 4A). The 625 nm output of the $Ru(dpp)_3Cl_2$ (Fig. 4B) is, correspondingly, the most intense in those areas. Overall, we observed that the UCP emissions are clearly robust enough to penetrate the overlying PCL+ $Ru(dpp)_3Cl_2$. The $Ru(dpp)_3Cl_2$ complex is uniformly dispersed throughout the fibers and is excited locally by the UCP-generated 480 nm light upon 980 nm excitation.

3.4 'Handshake' efficiency as a function of PCL + $Ru(dpp)_3Cl_2$ layer thickness

The layer of PCL + Y_2O_2S:Yb,Tm was maintained at ~90 μm thickness while the PCL + $Ru(dpp)_3Cl_2$ layer was varied (~9, 30, 90 and 270 μm). The difference of the four associated spectra in nitrogen and oxygen was assessed to determine the relative efficiency of each PCL + $Ru(dpp)_3Cl_2$ thickness in reporting local oxygen content. An example of such spectra is shown for an individual bilayer configuration (~90 μm PCL + Y_2O_2S:Yb,Tm/~30 μm PCL + $Ru(dpp)_3Cl_2$) under nitrogen and oxygen in Figure 5A. The intensity change due to the switching between the two atmospheres is clearly indicated by the difference in area between the two spectra.

By subtracting these spectra from each other, the oxygen-sensitive component of the emission can be isolated from the upconverting particle peaks (Figure 5B). Table 1 compares the different bilayer configurations by reporting the relative integrated intensities of oxygen-sensitive emission. The ~90 μm PCL + Y_2O_2S:Yb,Tm/~30 μm PCL + $Ru(dpp)_3Cl_2$ was found to yield the most efficient 'handshake' interaction. Therefore, all subsequent measurements were conducted using that specific set of layer thicknesses.

Also, in Figure 5B, the bilayer with as-is UCPs offered a more intense oxygen-sensitive emission than the corresponding bilayer containing ground and annealed particles. This difference in intensity was a result of the higher blue output from the as-received upconverting particles. The ground microparticles were heated at 550°C for 3 hours in an attempt to regain some of the intensity losses caused by defects introduced during the grinding step. Although the intensity of blue emission is lower, the smaller ground and annealed particles may impart better uniformity to the scaffold as a result of improved dispersion.

3.5 Gaseous oxygen sensing

Gaseous oxygen performance of the ~90 μm PCL + Y_2O_2S:Yb,Tm/~30 μm PCL + $Ru(dpp)_3Cl_2$ bilayer is shown in Figure 6. This plot was constructed according to the Stern-Volmer equation where I indicates the $Ru(dpp)_3Cl_2$ emission intensity, I_0 is the $Ru(dpp)_3Cl_2$ emission intensity in pure nitrogen, and K_{SV} symbolizes the Stern-Volmer quenching constant.

$$I_0/I = 1 + K_{SV}[O_2] \quad (1)$$

3.6 Response time

The response time of these bilayer samples was shown to be very rapid. The response from O_2 to N_2 was found to be 0.243±0.033 s, while the N_2 to O_2 response was found to be 0.118±0.016 s. Figure 7 shows the peak intensity of the oxygen-sensitive emission as the gas was cycled between oxygen and nitrogen. From this plot, we can see that the response is also shown to be entirely reversible.

3.7 Photobleaching

The photobleaching of the ~90 μm PCL + Y_2O_2S:Yb,Tm/~30 μm PCL + $Ru(dpp)_3Cl_2$ bilayer was assessed under blue light excitation in PBS. The decrease in the peak intensity was found to be ~1.5%, or within the variability of the source.

4. Discussion

Upconverter-driven energy transfer as a means of catalyzing optical or chemical changes is a relatively recent phenomenon.[36–40] Although most of this work has been with other luminescent indicators, Achatz *et al* investigated the use of UCPs for oxygen-sensing by incorporating upconverters and an oxygen-sensitive iridium (II) complex into an ethyl cellulose thin film.[38] The current state-of-the-art associated with the use of this 'handshake' interaction in sensing applications is in its infancy. In this work, we hypothesized that upconverting particles and an oxygen-sensitive complex could be used in a bilayer format to achieve oxygen sensing upon NIR light excitation. The bilayers were constructed of electrospun nanofibers to ensure rapid response times.

Although a single-layer format would have allowed for close proximity between the UCPs and oxygen-sensitive molecules and potentially greater 'handshake' efficiency, the bilayer format offers several advantages. The ability to excite the $Ru(dpp)_3Cl_2$ layer in transmission prevents UCPs from creating local limits to the $Ru(dpp)_3Cl_2$'s oxygen access or blocking/scattering the oxygen-sensitive output. Achatz *et al* attributed the decreased sensitivity and pronounced downward curvature of their sensor to the partial shielding of the Ir complex by the UCPs.[38] The bilayer format is also ideal for the incorporation of larger upconverting microparticles without interfering with the function of the oxygen-sensitive dye. Although it may be practically advantageous to use smaller upconverting nanoparticles in some applications, the upconversion efficiency of nanoparticles is much lower than their microparticle analogues.[41] The enhanced

surface-to-volume ratio of nanoparticles leads to surface deactivations and defects that limit their efficiency.[42] Therefore, there are clear advantages to using upconverting microparticles in applications in which sensor efficiency is more important than particle size.

These bilayer structures are constructed of a layer of PCL electrospun fiber containing the oxygen-sensitive complex $Ru(dpp)_3Cl_2$ on top of another layer of electrospun PCL containing Y_2O_2S:Yb,Tm upconverting microparticles. XRD showed that the crystalline Y_2O_2S:Yb,Tm UCPs were successfully incorporated into electrospun PCL (Fig. 2). Additionally, SEM demonstrated that the desired bilayer configuration (Fig. 3) was successfully achieved. EDS maps of yttrium and sulfur (Fig. 3B) confirm the presence of Y_2O_2S:Yb,Tm UCPs in only one of the layers as anticipated. We have shown that the desired oxygen sensing capabilities can be achieved upon NIR light excitation with such a bilayer configuration. When 980 nm NIR light contacts the PCL + Y_2O_2S:Yb,Tm side of the bilayer, it initiates a nonlinear multi-photon upconversion process (Fig. 1A) by which blue light (among other wavelengths) is produced. First, the sensitizer ion Yb^{3+} absorbs 980 nm photons via a $^2F_{5/2} \leftarrow ^2F_{7/2}$ transition. The activator ion Tm^{3+} then releases blue light via its $^1G_4 \rightarrow ^3H_6$ and $^1D_2 \rightarrow ^3F_4$ transitions.[43] This blue light emits from the first layer and is then absorbed by the second PCL + $Ru(dpp)_3Cl_2$ layer allowing for a metal-to-ligand charge transfer. Electrons from the *d* orbital of the Ru are excited to the ligand π^* orbital.[44] The resulting red phosphorescence is dynamically quenched by oxygen. This 'handshake' interaction was confirmed by confocal luminescence imaging (Fig 4) in which the 480 nm output of the agglomerated Y_2O_2S:Yb,Tm UCPs stimulates localized 625 nm output of $Ru(dpp)_3Cl_2$ following 980 nm excitation. Direct 980 nm stimulation of $Ru(dpp)_3Cl_2$-containing fiber does not result in 625 nm emission. This demonstrates both the 'handshake' and the fact that it depends on the presence of UCPs in a specific area. Despite its non-uniform distribution, the UCP blue emission is intense enough and the 'handshake' efficiency sufficiently high to successfully achieve accurate gaseous oxygen-sensing capabilities (Fig. 6) upon NIR excitation of the bilayer.

From the standpoint of Fig. 1B, incident NIR radiation excites the UCPs dispersed in the highly porous fiber layer. This results in a visible output of blue 480 nm emission in all directions. A significant fraction passes through the adjacent layer of PCL + $Ru(dpp)_3Cl_2$ fiber, resulting in a second emission at 625 nm. A fraction of that emerges from the face of the PCL + $Ru(dpp)_3Cl_2$ fiber layer and is detected by the spectrometer. This layer of fiber is also highly porous allowing efficient exchange and making it capable of rapidly sensing changes in local oxygen content.

Several features of the bilayer system were optimized to achieve maximum oxygen sensing capabilities. First, the thickness of the PCL + $Ru(dpp)_3Cl_2$ layer was varied while keeping the PCL + UCPs layer constant at ~90 μm. It was found that an ~30 μm layer achieved the maximum intensity of oxygen-sensitive output (Table 1). The lower intensity at ~9 μm thicknesses is a result of insufficient amounts of $Ru(dpp)_3Cl_2$ needed to capture blue UCP output and convert it into the oxygen-sensitive red phosphorescence. At PCL + $Ru(dpp)_3Cl_2$ layers thicker than 30 μm, we observed that the intensity of oxygen-sensitive emission begins to decrease once again. It is likely that the PCL +

$Ru(dpp)_3Cl_2$ fibers being excited most efficiently are those closest to the bilayer interface and that these red emissions then need to travel through additional fiber to reach the detector. Therefore, additional increases in $Ru(dpp)_3Cl_2$-containing layer thickness cause a decrease in net signal via absorption and scattering of the red emission. The red absorption of PCL itself is relatively low, so scattering is likely the dominant effect.[45] Additionally, the effect of switching the as-is UCPs for ground and annealed UCPs was assessed. Although the ground and annealed UCPs may be incorporated more uniformly and offer closer contact with the $Ru(dpp)_3Cl_2$, the brightest oxygen-sensitive output was achieved with the as-is UCPs (Fig. 5B). This observation is likely a result of decreased UCP emission from the mechanical grinding that could not be satisfactorily restored by annealing. This decrease in UCP emission is likely dominated by the introduction of defects as a result of grinding and may also result partially from decreased particle size.

Additionally, most polymer sensors are constructed from polymer films, but in oxygen sensing applications, film carriers suffer from delayed response times as a result of their 2D geometry.[46] We have previously shown that nanofibers greatly reduce the response time of oxygen-sensitive molecules as a result of their inherently small diffusion distances and substantially increased surface-to-volume ratio, which combine to greatly increase the rate of oxygen exchange.[46] Therefore, by constructing the bilayer sensor out of electrospun layers, we were able to achieve extremely rapid response times (N_2 to O_2: 0.118±0.016 s; O_2 to N_2: 0.243±0.033 s;) as demonstrated from Fig. 7. Note that the actual response is likely limited by mechanical factors (i.e., the time it takes to fully exchange the gas in the cuvette). Therefore, the actual response times are probably even shorter than those observed here. Other advantages of using electrospun nanofibers include a thin and flexible format that can be easily manipulated and miniaturized.

Incorporation of $Ru(dpp)_3Cl_2$ into electrospun PCL nanofiber layers achieved a quasi-linear Stern-Volmer response (Fig. 6), where the term quasi-linear is used since the fit does not cross the y-axis at 1. This approximately linear response (R^2 of 0.96) indicates that the probe was homogenously incorporated into the fibers similar to the linear responses we have observed previously[46–48]. A linear response provides for simplicity of measurement and is advantageous over the commonly observed downward curvature of film-based sensors analytically described using more complex models.[49]

The effects of photobleaching were minor. As was previously observed [31], good dispersion of the $Ru(dpp)_3Cl_2$ resulting from the speed of the electrospinning process decreases complex agglomeration and thus photobleaching. However, we have previously observed that using polyethersulfone (PES) instead of PCL as the polymer matrix greatly reduces the rate of photobleaching for $Ru(dpp)_3Cl_2$.[46] Therefore, future bilayers could be constructed out of a different polymer host to reduce the rate of photobleaching. However, PES alone can be difficult to electrospin and is not as biocompatible as PCL. Therefore, core-shell electrospun nanofibers could be constructed using a coaxial needle. This configuration could allow for a PES + $Ru(dpp)_3Cl_2$ core to reduce photobleaching and a PCL shell to maintain good biocompatibility. Additionally, we have previously shown that such a core-shell structure can mitigate concerns with dye leakage.[50] However, even PCL+$Ru(dpp)_3Cl_2$ were found to not exhibit cytotoxic

effects to migrating tumor cells.[46]

For future studies utilizing this upconverter-powered bilayer sensor, we plan to investigate the detection of hypoxic regions of U251 human glioblastoma cell aggregates by the $Ru(dpp)_3Cl_2$-containing layer. The bilayer will be excited in transmission from the UCP-containing side. PDMS-based tissue phantoms will be placed in front of the NIR excitation source to assess the possibility for quantitative *in vivo* sensing. To prevent the effects on output intensity due to small temperature variations, setup configuration, light source variability, etc., we plan to employ ratiometric sensing based on the relatively bright 800 nm emission from the upconverting particles.

5. Conclusions

In numerous biomedical applications, the ability to sense and report localized oxygen concentration is desired. Here, we used upconverting particles to potentially overcome the traditional absorption and scattering barriers associated with biological tissues by using 980 nm light to cause the Y_2O_2S:Yb,Tm upconverter to emit blue light. An adjacent layer of fibers containing $Ru(dpp)_3Cl_2$ on top of a layer of the fibers containing UCPs utilized this NIR-stimulated blue emission to exhibit quantifiable sensitivity to ambient levels of molecular oxygen. Confocal microscopy verified that the desired conversions were taking place on a localized scale. A layer of UCP-containing fiber ~90 μm thick combined with a ~30 μm $Ru(dpp)_3Cl_2$-containing layer was found to yield the most efficient interaction. A quasi-linear linear Stern-Volmer response was achieved along with an absence of significant photobleaching.

6. Acknowledgements

KP acknowledges the generous support of the Department of Defense (DoD) through the National Defense Science & Engineering Graduate Fellowship (NDSEG) Program. This work was supported by research grants from the United States National Science Foundation under Grant Nos. CBET-1033991 and EEC-0425626. We gratefully acknowledge the use of the Leica SP5 Confocal/MultiPhoton microscope within the UCSD School of Medicine Microscopy Core under the auspices of the NINDS P30 core grant (NS047101) Any opinions, findings, and conclusions or recommendations expressed in this material are those of the authors and do not necessarily reflect the views of the National Science Foundation or the National Institutes of Health. There is no competing interest by the authors.

Figure and Table Captions

Figure 1: (A) Combined energy level diagrams for Y_2O_2S:Yb,Tm upconverting particles and oxygen-sensitive $Ru(dpp)_3Cl_2$, demonstrating the nature of the optoelectronic 'handshake' (B) Conversion processes within a representative bilayer configuration.

Figure 2: XRD patterns for PCL electrospun fibers containing as-is and ground and annealed Y_2O_2S:Yb,Tm microparticles. The inset graph shows the XRD patterns for the as-is and ground and annealed Y_2O_2S:Yb,Tm powders.

Figure 3: Representative bilayer interface (A) secondary electron SEM image and (B) EDS map. Upconverting particle layer (C) secondary electron SEM image and (D) backscattered electron SEM image.

Figure 4: PMT results of bilayer specimen tested under vacuum showing (A) 480 nm output of Y_2O_2S:Yb,Tm UCPs upon 980 nm excitation (grey scale) image (B) 625 nm output of $Ru(dpp)_3Cl_2$ during the 980 nm excitation. The 625 nm output of the $Ru(dpp)_3Cl_2$-containing fiber is at its greatest intensity/co-localized to the area of 480 nm output from the aggregated Y_2O_2S:Yb,Tm UCPs.

Figure 5: (A) Emission spectra of ~90 μm PCL + Y_2O_2S:Yb,Tm/~30 μm PCL + $Ru(dpp)_3Cl_2$ bilayer in nitrogen and oxygen (B) Subtracted nitrogen and oxygen spectra for ~90 μm PCL + Y_2O_2S:Yb,Tm/~30 μm PCL + $Ru(dpp)_3Cl_2$ bilayers made using as-received UCPs (upper line) and ground and annealed UCPs.

Table 1: 'Handshake' efficiency of different bilayer configurations as shown by relative integrated intensities of oxygen-sensitive emission.

Figure 6: Gaseous oxygen sensing for ~90 μm PCL + Y_2O_2S:Yb,Tm/~30 μm PCL + $Ru(dpp)_3C_2$ bilayer.

Figure 7: The response of ~90 μm PCL + Y_2O_2S:Yb,Tm/~30 μm PCL + $Ru(dpp)_3Cl_2$ bilayer to alternating exposures to N_2 and O_2 gas.

References

[1] J. Lopez-Barneo, R. Pardal, P. Ortega-Sáenz, Cellular mechanism of oxygen sensing., Annu. Rev. Physiol. 63 (2001) 259–287. doi:10.1146/annurev.physiol.63.1.259.

[2] R. Portner, O.B.J. Platas Barradas, Cultivation of mammalian cells in fixed-bed reactors, 2nd ed., Humana Press, New York, 2007.

[3] L. Liu, B. Li, R. Qin, H. Zhao, X. Ren, Z. Su, Synthesis and characterization of new bifunctional nanocomposites possessing upconversion and oxygen-sensing properties., Nanotechnology. 21 (2010) 285701. doi:10.1088/0957-4484/21/28/285701.

[4] R. Xue, M.T. Nelson, S.A. Teixeira, M.S. Viapiano, J.J. Lannutti, Cancer cell aggregate hypoxia visualized in vitro via biocompatible fiber sensors, Biomaterials. 76 (2016) 208–217. doi:10.1016/j.biomaterials.2015.10.055.

[5] X. Luo, W. Cao, Blue, green, red upconversion luminescence and optical characteristics of rare earth doped rare earth oxide and oxysulfide, Sci. China, Ser. B Chem. 50 (2007) 505–513. doi:10.1007/s11426-007-0067-z.

[6] X.D. Wang, H.X. Chen, Y. Zhao, X. Chen, X.R. Wang, X. Chen, Optical oxygen sensors move towards colorimetric determination, TrAC - Trends Anal. Chem. 29 (2010) 319–338. doi:10.1016/j.trac.2010.01.004.

[7] Y. Amao, Probes and polymers for optical sensing of oxygen, Microchim. Acta. 143 (2003) 1–12. doi:10.1007/s00604-003-0037-x.

[8] O.S. Wolfbeis, Luminescent sensing and imaging of oxygen: Fierce competition to the Clark electrode, BioEssays. 37 (2015) 921–928. doi:10.1002/bies.201500002.

[9] S.W. Lai, Y.J. Hou, C.M. Che, H.L. Pang, K.Y. Wong, C.K. Chang, et al., Electronic spectroscopy, photophysical properties, and emission quenching studies of an oxidatively robust perfluorinated platinum porphyrin, Inorg. Chem. 43 (2004) 3724–3732. doi:10.1021/ic049902h.

[10] P.J. Spellane, M. Gouterman, a. Antipas, S. Kim, Y.C. Liu, Porphyrins. 40. Electronic spectra and four-orbital energies of free-base, zinc, copper, and palladium tetrakis(perfluorophenyl)porphyrins, Inorg. Chem. 19 (1980) 386–391. doi:10.1021/ic50204a021.

[11] P.C. Alford, M.J. Cook, A.P. Lewis, G.S.G. McAuliffe, V. Skarda, A.J.. Thomson, et al., Luminescent metal complexes. Part 5. Luminescence properties of ring-substituted 1,10-phenanthroline tris-complexes of ruthenium(II), J. Chem. Soc. Perkin Trans. 2. (1985) 705–709.

[12] M. Bossi, M. Daraio, P. Aramendía, Luminescence quenching of Ru (II) complexes in polydimethylsiloxane sensors for oxygen, J. Photochem. …. 120 (1999) 15–21. doi:10.1016/S1010-6030(98)00418-3.

[13] Y. Amao, I. Okura, H. Shinohara, H. Nishide, An Optical Sensing Material for Trace Analysis of Oxygen. Metalloporphyrin Dispersed in Poly(1-trimethylsilyl-1-propyne) Film, Polym. J. 34 (2002) 411–417. doi:10.1295/polymj.34.411.

[14] S.-K. Lee, I. Okura, Photostable Optical Oxygen Sensing Material: Platinum Tetrakis(pentafluorophenyl)porphyrin Immobilized in Polystyrene, Anal. Commun. 34 (1997) 185–188. doi:10.1039/a701130j.

[15] S.M. Borisov, I. Klimant, Ultrabright oxygen optodes based on cyclometalated iridium(III) coumarin complexes, Anal. Chem. 79 (2007) 7501–7509. doi:10.1021/ac0710836.

[16] P. Zhang, H. Huang, Y. Chen, J. Wang, L. Ji, H. Chao, Ruthenium(II) anthraquinone complexes as two-photon luminescent probes for cycling hypoxia imaging invivo, Biomaterials. 53 (2015) 522–531. doi:10.1016/j.biomaterials.2015.02.126.

[17] X. Wang, D.E. Achatz, C. Hupf, M. Sperber, J. Wegener, S. Bange, et al., Imaging of cellular oxygen via two-photon excitation of fluorescent sensor nanoparticles, Sensors Actuators B Chem. 188 (2013) 257–262. doi:10.1016/j.snb.2013.06.087.

[18] R.I. Dmitriev, A. V. Kondrashina, K. Koren, I. Klimant, A. V. Zhdanov, J.M.P. Pakan, et al., Small molecule phosphorescent probes for O2 imaging in 3D tissue models, Biomater. Sci. 2 (2014) 853. doi:10.1039/c3bm60272a.

[19] H. Kurokawa, H. Ito, M. Inoue, K. Tabata, Y. Sato, K. Yamagata, et al., High resolution imaging of intracellular oxygen concentration by phosphorescence lifetime., Sci. Rep. 5 (2015) 10657. doi:10.1038/srep10657.

[20] T. Yoshihara, S. Murayama, S. Tobita, Ratiometric molecular probes based on dual emission of a blue fluorescent coumarin and a red phosphorescent cationic iridium(III) complex for intracellular oxygen sensing, Sensors (Switzerland). 15 (2015) 13503–13521. doi:10.3390/s150613503.

[21] X. Zheng, X. Wang, H. Mao, W. Wu, B. Liu, X. Jiang, Hypoxia-specific ultrasensitive detection of tumours and cancer cells in vivo, Nat. Commun. 6 (2015) 5834. doi:10.1038/ncomms6834.

[22] C.L. Tsai, J.C. Chen, W.J. Wang, Near-infrared absorption property of biological soft tissue constituents, J. Med. Biol. Eng. 21 (2001) 7–14.

[23] R.R. Anderson, J.A. Parrish, The optics of human skin., J. Invest. Dermatol. 77 (1981) 13–19. doi:10.1111/1523-1747.ep12479191.

[24] G.M. Hale, M.R. Querry, Optical constants of water in the 200-nm to 200-micron wavelength region., Appl. Opt. 12 (1973) 555–563. doi:10.1364/AO.12.000555.

[25] L.A. Sordillo, Y. Pu, S. Pratavieira, Y. Budansky, R.R. Alfano, Deep optical imaging of tissue using the second and third near-infrared spectral windows., J. Biomed. Opt. 19 (2014) 056004. doi:10.1117/1.JBO.19.5.056004.

[26] L. Cheng, C. Wang, Z. Liu, Upconversion nanoparticles and their composite nanostructures for biomedical imaging and cancer therapy, Nanoscale. (2012) 23–37. doi:10.1039/c2nr32311g.

[27] D.K. Chatterjee, M.K. Gnanasammandhan, Y. Zhang, Small upconverting fluorescent nanoparticles for biomedical applications, Small. 6 (2010) 2781–2795. doi:10.1002/smll.201000418.

[28] K. Szaciłowski, W. Macyk, A. Drzewiecka-Matuszek, M. Brindell, G. Stochel, Bioinorganic photochemistry: frontiers and mechanisms, Chem. Rev. 105 (2005) 2647–2694. doi:10.1021/cr030707e.

[29] F.L. Arbeloa, P.R. Ojeda, I.L. Arbeloa, Flourescence self-quenching of the molecular forms of Rhodamine B in aqueous and ethanolic solutions, J. Lumin. 44 (1989) 105–112. doi:10.1016/0022-2313(89)90027-6.

[30] R.M. Clegg, Fluorescence resonance energy transfer, Curr. Opin. Biotechnol. 6 (1995) 103–110. doi:10.1016/0958-1669(95)80016-6.

[31] J.Y. Chiu, C.M. Yu, M.J. Yen, L.C. Chen, Glucose sensing electrodes based on a poly(3,4-ethylenedioxythiophene)/Prussian blue bilayer and multi-walled carbon nanotubes, Biosens. Bioelectron. 24 (2009) 2015–2020. doi:10.1016/j.bios.2008.10.010.

[32] W.P. Jakubik, Hydrogen gas-sensing with bilayer structures of WO3 and Pd in SAW and electric systems, Thin Solid Films. 517 (2009) 6188–6191. doi:10.1016/j.tsf.2009.04.008.

[33] D.-J. Yao, Y.-R. Yang, C.-C. Tai, W.-H. Hsiao, Y.-C. Ling, A biochemical sensing system using an 11-MUA/calix[6]arene bilayer to sense amine vapors, J. Micromechanics Microengineering. 17 (2007) 1435–1441. doi:10.1088/0960-1317/17/8/004.

[34] J. Gaumer, A. Prasad, D. Lee, J. Lannutti, Structure-function relationships and source-to-ground distance in electrospun polycaprolactone, Acta Biomater. 5 (2009) 1552–1561. doi:10.1016/j.actbio.2009.01.021.

[35] J. Nam, Y. Huang, S. Agarwal, J. Lannutti, Materials selection and residual solvent retention in biodegradable electrospun fibers, J. Appl. Polym. Sci. 107 (2008) 1547–1554. doi:10.1002/app.27063.

[36] J. Liu, Y. Liu, W. Bu, J. Bu, Y. Sun, J. Du, et al., Ultrasensitive nanosensors based on upconversion nanoparticles for selective hypoxia imaging in vivo upon near-infrared excitation, J. Am. Chem. Soc. 136 (2014) 9701–9709. doi:10.1021/ja5042989.

[37] R.J. Meier, J.M.B. Simbuürger, T. Soukka, M. Schaüferling, Background-free referenced luminescence sensing and imaging of pH using upconverting phosphors and color camera read-out, Anal. Chem. 86 (2014) 5535–5540. doi:10.1021/ac5009207.

[38] D.E. Achatz, R.J. Meier, L.H. Fischer, O.S. Wolfbeis, Luminescent sensing of oxygen using a quenchable probe and upconverting nanoparticles, Angew. Chemie - Int. Ed. 50 (2011) 260–263. doi:10.1002/anie.201004902.

[39] R. Ali, S.M. Saleh, R.J. Meier, H.A. Azab, I.I. Abdelgawad, O.S. Wolfbeis, Upconverting nanoparticle based optical sensor for carbon dioxide, Sensors Actuators, B Chem. 150 (2010) 126–131. doi:10.1016/j.snb.2010.07.031.

[40] L.-N. Sun, H. Peng, M.I.J. Stich, D. Achatz, O.S. Wolfbeis, pH sensor based on upconverting luminescent lanthanide nanorods., Chem. Commun. (Camb). (2009) 5000–5002. doi:10.1039/b907822c.

[41] X. Li, F. Zhang, D. Zhao, Highly efficient lanthanide upconverting nanomaterials: Progresses and challenges, Nano Today. 8 (2013) 643–676. doi:10.1016/j.nantod.2013.11.003.

[42] F. Wang, J. Wang, X. Liu, Direct evidence of a surface quenching effect on size-dependent luminescence of upconversion nanoparticles, Angew. Chemie - Int. Ed. 49 (2010) 7456–7460. doi:10.1002/anie.201003959.

[43] S. Heer, K. Kömpe, H.U. Güdel, M. Haase, Highly efficient multicolour upconversion emission in transparent colloids of lanthanide-doped NaYF4 nanocrystals, Adv. Mater. 16 (2004) 2102–2105. doi:10.1002/adma.200400772.

[44] M. Quaranta, S.M. Borisov, I. Klimant, Indicators for optical oxygen sensors, Bioanal. Rev. 4 (2012) 115–157. doi:10.1007/s12566-012-0032-y.

[45] Sigma-Aldrich, Polycaprolactone: FTIR, (n.d.). http://www.sigmaaldrich.com/spectra/ftir/FTIR002053.PDF (accessed September 4, 2015).

[46] R. Xue, P. Behera, M.S. Viapiano, J.J. Lannutti, Rapid response oxygen-sensing nanofibers, Mater. Sci. Eng. C. 33 (2013) 3450–3457. doi:10.1016/j.msec.2013.04.030.

[47] R. Xue, P. Behera, J. Xu, M.S. Viapiano, J.J. Lannutti, Polydimethylsiloxane core-polycaprolactone shell nanofibers as biocompatible, real-time oxygen sensors, Sensors Actuators, B Chem. 192 (2014) 697–707. doi:10.1016/j.snb.2013.10.084.

[48] R. Xue, C. Ge, K. Richardson, A. Palmer, M. Viapiano, J.J. Lannutti, Microscale sensing of oxygen via encapsulated porphyrin nanofibers: effect of indicator and polymer “core” permeability, ACS Appl. Mater. Interfaces. 7 (2015) 8606–8614. doi:10.1021/acsami.5b00403.

[49] E.R. Carraway, J.N. Demas, B.A. Degraff, Luminescence quenching mechanism for microheterogeneous systems, Anal. Chem. 63 (1991) 332–336.

[50] R. Xue, Nanofiber Based Optical Sensors for Oxygen Determination, Ohio State University, 2014.

PCL + UCPs Layer Thickness [µm]	PCL + Ru(dpp)Cl Layer Thickness [µm]	Relative Integrated Intensity of Oxygen-Sensitive Emission
~90	~9	0.407
~90	~30	1.000
~90	~90	0.827
~90	~270	0.717

A

B

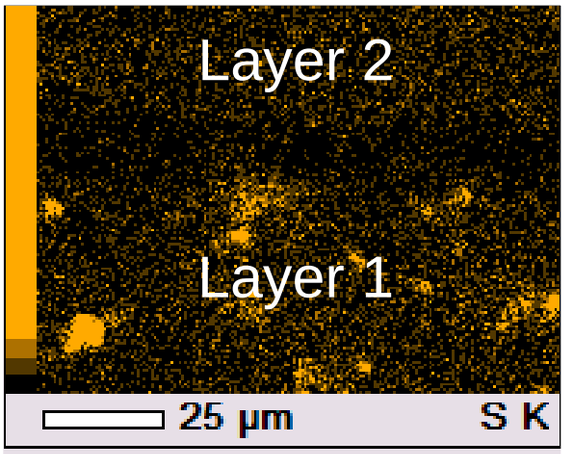
Layer 2
Layer 1
25 µm
S K

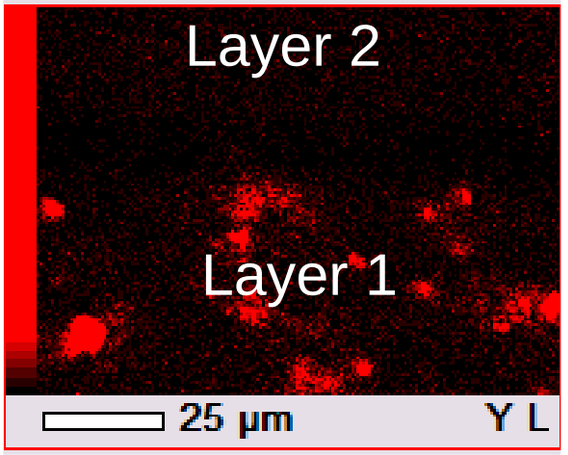
Layer 2
Layer 1
25 µm
Y L

C

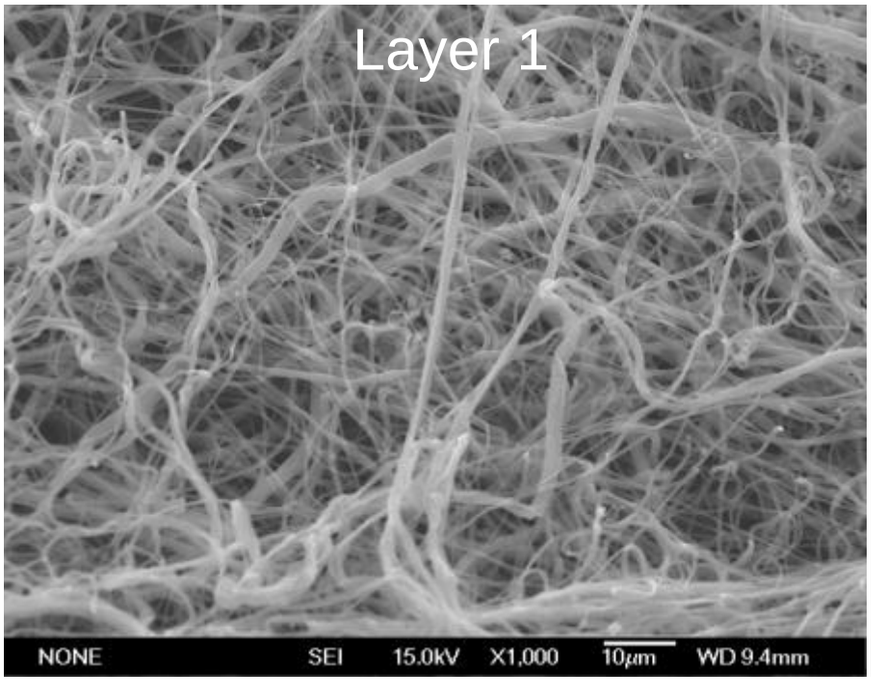
Layer 1
NONE
SEI
15.0kV
X1,000
10µm
WD 9.4mm

D

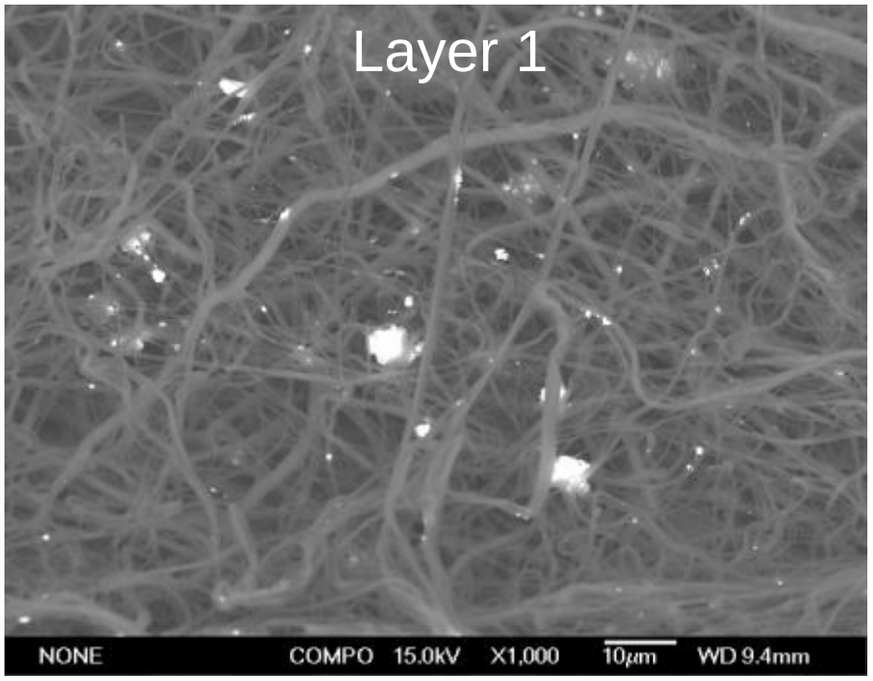
Layer 1
NONE
COMPO
15.0kV
X1,000
10µm
WD 9.4mm

A

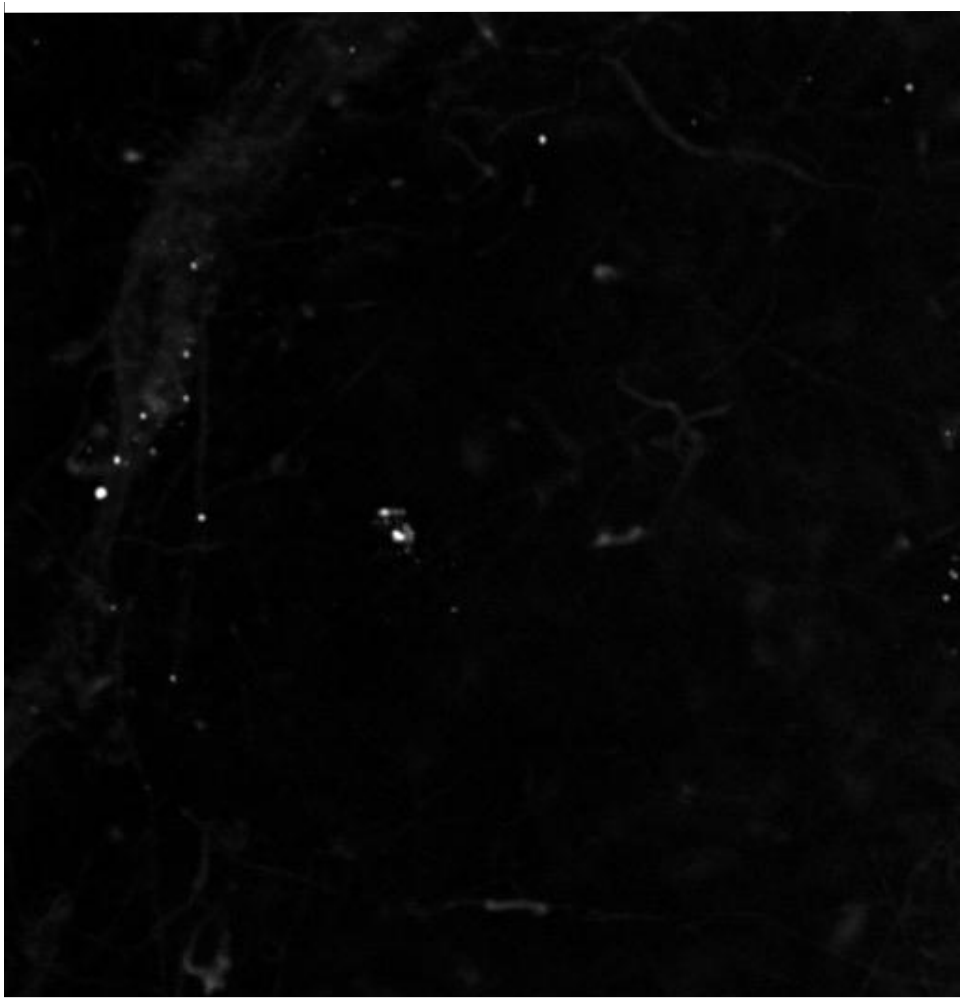

B

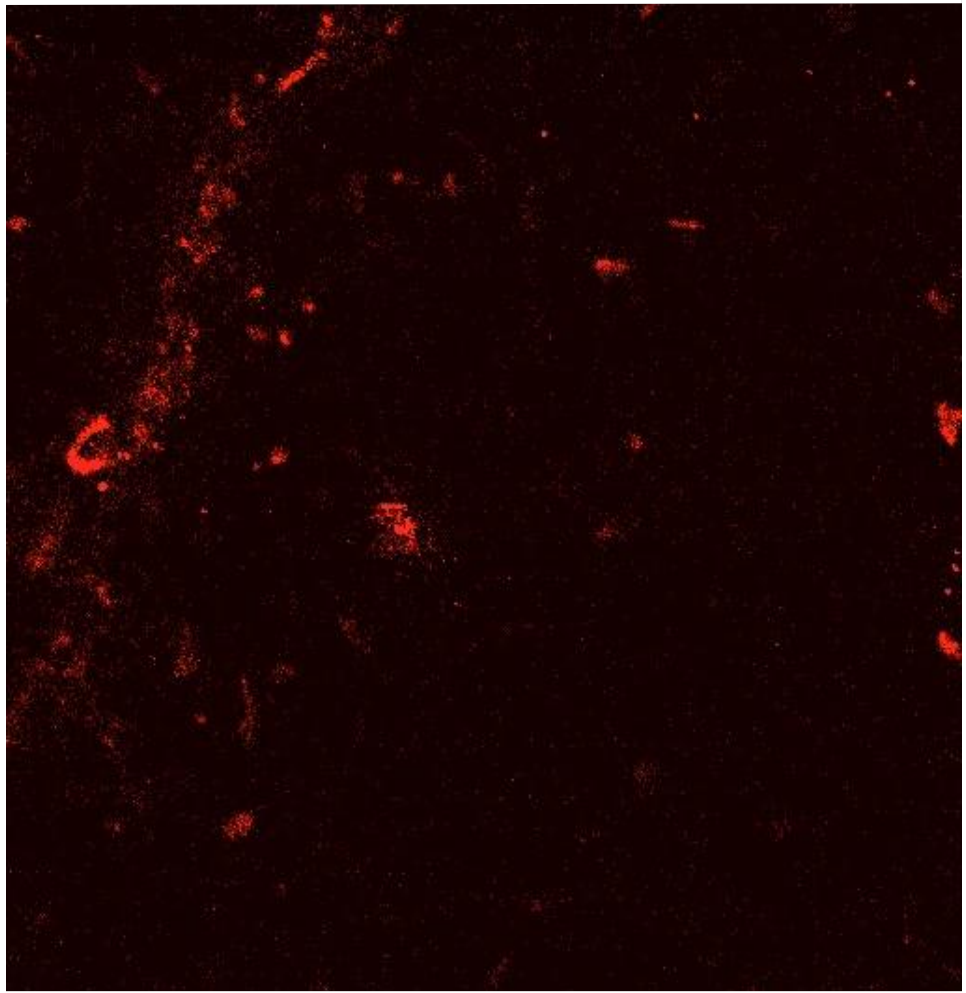

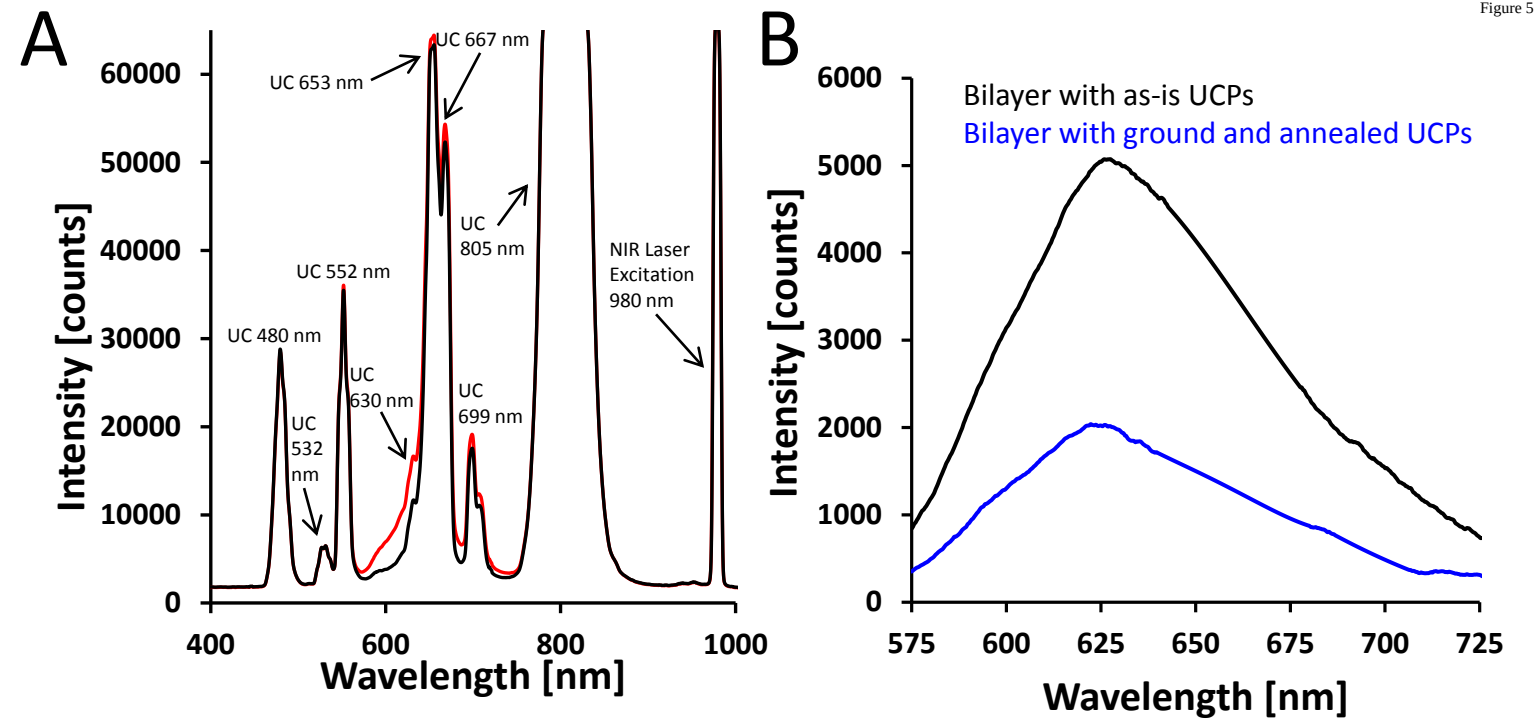
A
Intensity [counts]
Wavelength [nm]
UC 480 nm
UC 532 nm
UC 552 nm
UC 630 nm
UC 653 nm
UC 667 nm
UC 699 nm
UC 805 nm
NIR Laser Excitation 980 nm
B
Intensity [counts]
Wavelength [nm]
Bilayer with as-is UCPs
Bilayer with ground and annealed UCPs

Figure 6

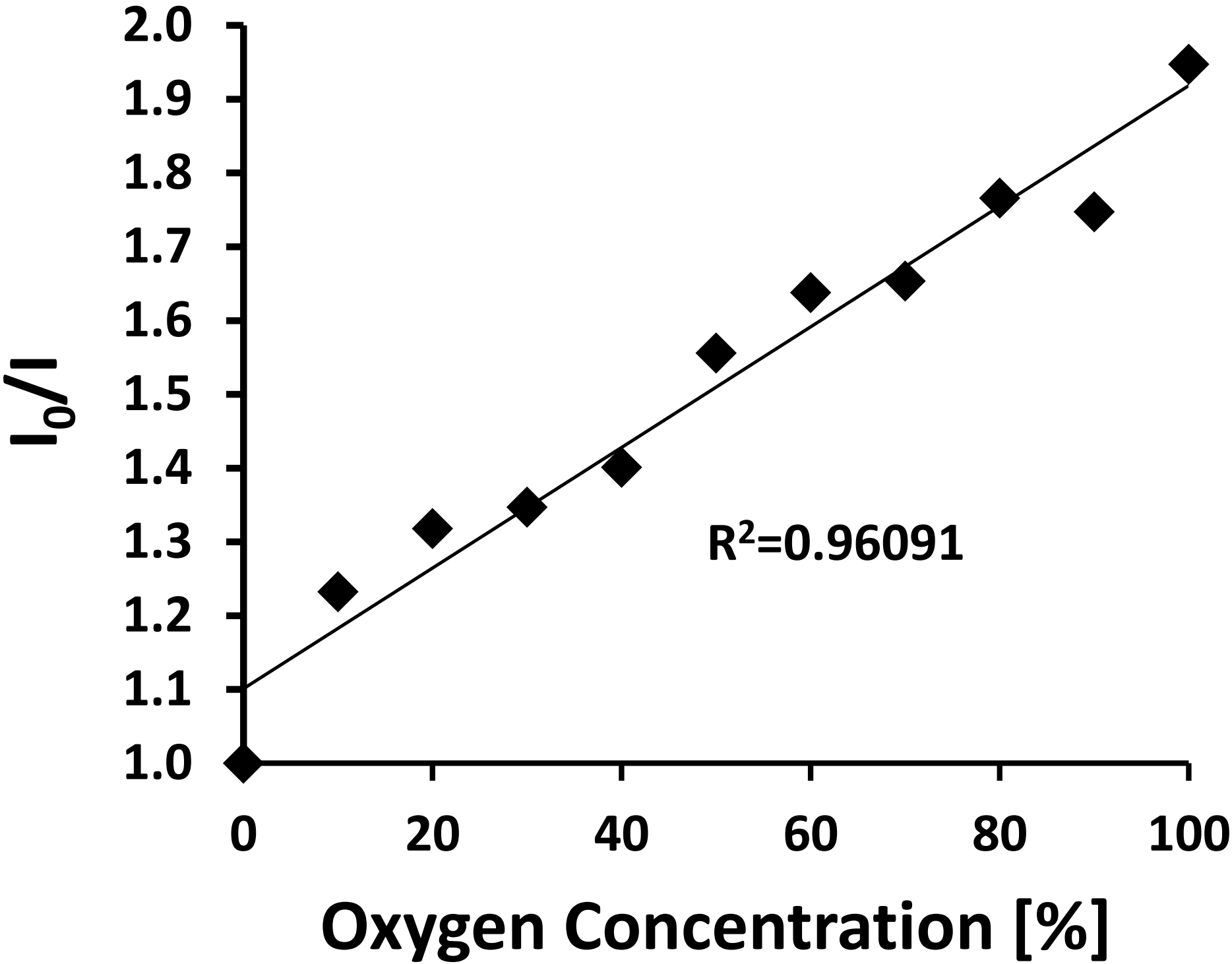
2.0
1.9
1.8
1.7
1.6
1.5
1.4
1.3
1.2
1.1
1.0
I_0/I
R^2=0.96091
0
20
40
60
80
100
Oxygen Concentration [%]

Figure 7

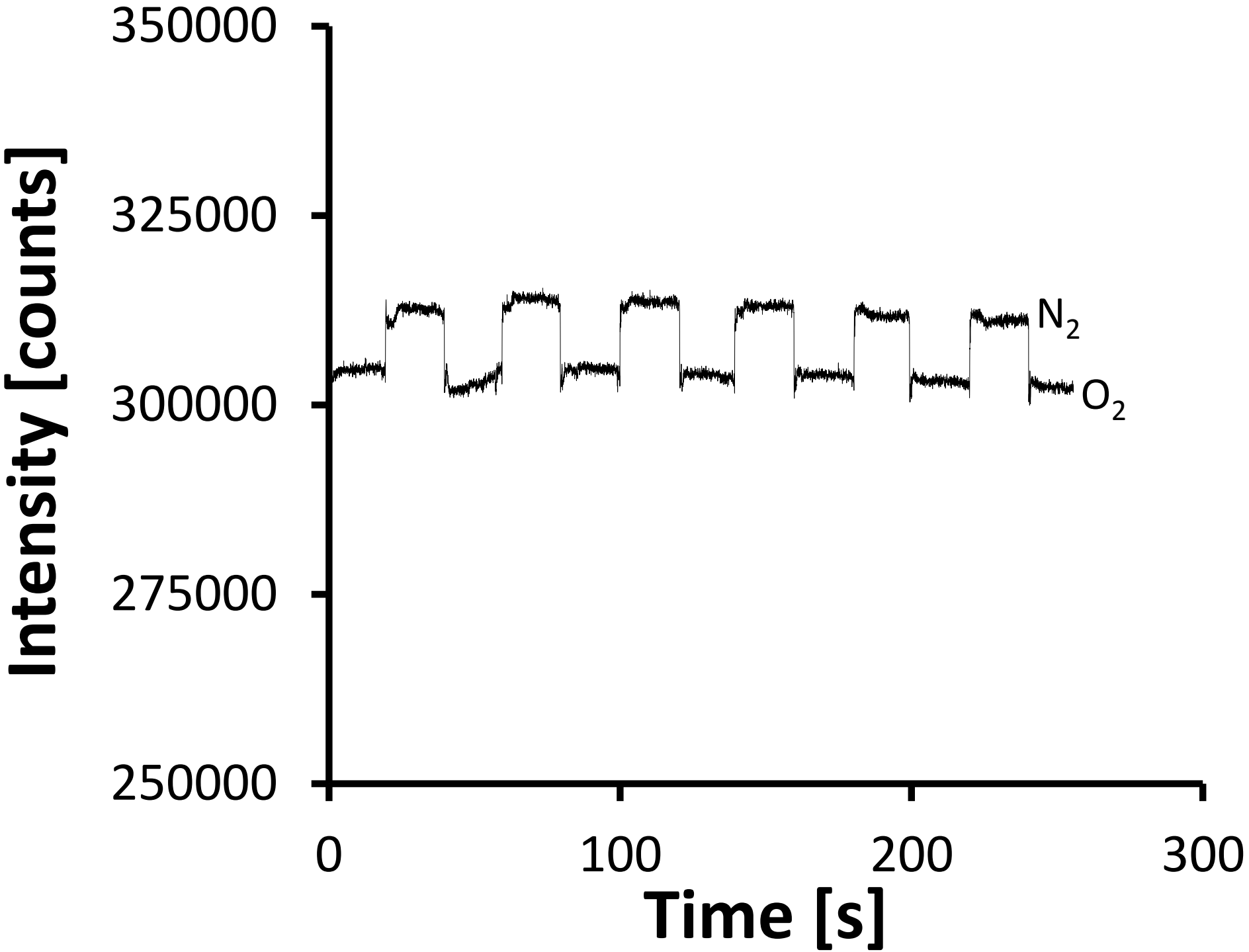
350000
325000
300000
275000
250000
Intensity [counts]
0
100
200
300
Time [s]
N2
O2

Kayla F. Presley received her BS degree from The Ohio State University (Columbus, Ohio) in 2013. She is currently a National Defense Science and Engineering Graduate (NDSEG) Fellow and PhD candidate in Materials Science and Engineering at Ohio State. Her research is focused on the development of optical-based nanofiber sensors, particularly the advancement of such sensors across a range of biomedical applications.

Soshan Cheong is currently a postdoctoral fellow at the University of New South Wales, Australia. She received her PhD in Chemistry (2010) from Victoria University of Wellington, New Zealand. Under the supervision of Professor Richard D. Tilley, she used electron microscopy to study the solution-phase synthesis and growth of nanoparticles for applications in catalysis and biomedicine. Her current research focuses on the controlled synthesis of catalytically active nanoparticles, with a particular emphasis on *in situ* characterization and growth mechanisms of shaped nanoparticles.

Alex Cochran is currently an undergraduate researcher in the Lannutti laboratory working towards his BS in Materials Science and Engineering at The Ohio State University. His interests include biologically compatible materials and their usefulness concerning improving patient care. He hopes to continue his work via a Master's degree.

Richard D. Tilley is the Director of Electron Microscope Unit and in the School of Chemistry at University of New South Wales (UNSW) in Sydney Australia. Before UNSW he was with the School of Chemical and Physical sciences at Victoria University of Wellington in New Zealand. His research is focused on solution synthesis and electron microscopy characterization of nanoparticles and quantum dots for applications ranging from catalysis to biomedical imaging. He obtained his PhD in the Department of Chemistry, University of Cambridge, UK, after which he was a Postdoctoral Fellow for 2 years at the Toshiba Basic R&D Center, Japan.

Josh E. Collins is Chief Technology Officer and co-founder of Intelligent Material Solutions, Inc. Mr. Collins has been synthesizing phosphors and nanophosphors for over 10 years and has developed methods for scalable synthesis of rare earth doped nanocrystals. He has developed custom optical materials for a broad variety of government and commercial applications. Mr. Collins holds a Guest Researcher appointment at the NIBIB, NIH and has been published in numerous peer-reviewed journals. He obtained his Bachelor's of Science from King's College (PA) in 2001.

John J. Lannutti is a Professor of Materials Science and Engineering within The Ohio State University (Columbus, Ohio). He received his BS and MS degrees in Materials Science and Engineering from the University of Florida in 1982 and 1984, respectively. He worked for Alzeta Corporation in Silicon Valley from 1984 to 1987 before receiving his PhD in Materials Science and Engineering from the University of Washington (Seattle) in 1990. His main research interests are 'smart' nanofibers as chemical and optical sensors and highly engineered release vehicles for contraceptive applications. He has authored >200 articles in refereed journals and 8 patents.